Published in final edited form as:

Annu Rev Biomed Eng. 2014 July 11; 16: 53–76. doi:10.1146/annurev-bioeng-071813-104517.

Computational Modeling of Cardiac Valve Function and Intervention

Wei Sun, **Caitlin Martin**, and **Thuy Pham**

Tissue Mechanics Lab, The Wallace H. Coulter Department of Biomedical Engineering, Georgia Institute of Technology, Atlanta, Georgia 30313

Abstract

In the past two decades, major advances have been made in the clinical evaluation and treatment of valvular heart disease owing to the advent of noninvasive cardiac imaging modalities. In clinical practice, valvular disease evaluation is typically performed on two-dimensional (2D) images, even though most imaging modalities offer three-dimensional (3D) volumetric, time-resolved data. Such 3D data offer researchers the possibility to reconstruct the 3D geometry of heart valves at a patient-specific level. When these data are integrated with computational models, native heart valve biomechanical function can be investigated, and preoperative planning tools can be developed. In this review, we outline the advances in valve geometry reconstruction, tissue property modeling, and loading and boundary definitions for the purpose of realistic computational structural analysis of cardiac valve function and intervention.

Keywords

heart valve; finite element analysis; cardiac imaging; aortic valve; mitral valve

1. INTRODUCTION

1.1. Heart Valve Structure and Function

The heart has four cardiac valves—namely, the aortic, mitral, tricuspid, and pulmonic valves—which control unidirectional blood flow through the heart during the cardiac cycle. These four valves are primarily passive structures; that is, they open and close based on the differential blood pressure on each side of the valve leaflets. Diseases of the aortic and mitral valves, on the left side of the heart, are much more prevalent than those of the tricuspid and pulmonic valves, on the right, and consequently, computational studies of valve function have been centered mainly on the aortic and mitral valves. For this reason, this review focuses on studies related to the aortic and mitral valves, although modeling approaches discussed herein could be applied to the pulmonary and tricuspid valves as well.

DISCLOSURE STATEMENT

The authors are not aware of any affiliations, memberships, funding, or financial holdings that might be perceived as affecting the objectivity of this review.

In order to construct a realistic valve model and simulate deformation and flow during the cardiac cycle, it is important to have a good understanding of the healthy normal valve anatomy and the associated structure–function relationships, which we briefly summarize in the following sections.

1.1.1. Aortic valve—The aortic valve (AV) consists of three leaflets: the left coronary, right coronary, and noncoronary leaflets (Figure 1*a*). These three leaflets may differ in size and are not necessarily symmetrically aligned (spaced 120° apart from each other) (1). Microscopically, each leaflet is composed of three layers: ventricularis, spongiosa, and fibrosa. Each layer contains a different amount of elastin, collagen, glycosaminoglycans, and proteoglycans. This complex structure results in highly complex material properties, with each layer displaying a distinct nonlinear, anisotropic response (2). Nonetheless, for modeling convenience, the leaflets are often treated as a single-layer, homogeneous material in computational models (3–13). The subvalvular and surrounding structures are less studied in the literature; however, inclusion of these surrounding tissues in computational models allows for more realistic boundary conditions, particularly for patient-specific modeling of valve function.

Briefly, the AV (i.e., leaflets) resides within the aortic root, which is defined as the portion of the left ventricular outflow tract delineated by the sinotubular junction (STJ) superiorly and the valve annulus inferiorly (Figure 1*b*). The aortic annulus is not a simple, clearly defined, homogeneous structure. One-third of the annulus is composed primarily of fibrous tissue, which is located partially below the noncoronary and left coronary leaflets in continuity with the anterior mitral leaflet. The thickened portions of fibrous tissue between the leaflets, referred to as the fibrous trigones, mechanically reinforce the annulus. The remaining two-thirds of the annulus is composed of ventricular muscle (Figure 1*a*). The aortic annulus is an important anatomic structure for anchoring current transcatheter aortic valves (TAVs). As the fibrous tissue is much stronger than the ventricular muscle, aortic rupture is not expected to occur at the fibrous region during the TAV procedure. Distal to the annulus are the three sinuses of Valsalva (SOV), specifically the left coronary, right coronary, and noncoronary sinuses, which are the bulged portions of the aortic root. Distally, the aortic sinuses are connected to the ascending aorta at the STJ. The leaflets, sinuses, and ascending aorta have distinct material properties, with the ascending aorta being significantly more compliant than the sinuses (14, 15) and more isotropic than the leaflets (14, 16). It is thus important to include accurate definitions of these structures and regional material properties in computational models.

1.1.2. Mitral valve—The mitral valve (MV) is a complex yet elegantly structured cardiac valve that consists of an annulus, two leaflets, approximately 25 chordae tendineae, two papillary muscles, and the underlying left ventricular myocardium (Figure 1*c*). The mitral annulus (MA), similar to the aortic annulus, is subdivided into a lateral (anterior) portion, composed mainly of cardiac muscle, and a septal (posterior) portion, composed of fibrous tissue. The anterior mitral leaflet (AML) is connected to the AV via the aortic-mitral curtain, and the posterior mitral leaflet (PML) is hinged on the posterior MA (Figure 1*d*). Microscopically, the leaflets are composed of multiple layers—namely, the atrialis,

spongiosa, fibrosa, and ventricularis. However, like the AV leaflets, the MV leaflets are often modeled as a single-layer structure in computational models (17–19). The fibrous chords are composed mainly of collagen bundles, which give the chords high stiffness and maintain minimal extension to prevent the leaflets from pillowing into the left atrium during systole. The chords originate from either the two major papillary muscles (on the anterolateral and posterolateral walls) or multiple small muscle bundles attaching to the ventricular wall. Normal MV function involves a proper force balance, with each of its components working congruently during a cardiac cycle. Pathological alterations affecting any of the components, such as chord rupture (20), annulus dilatation (21), papillary muscle displacement (22, 23), leaflet calcification, and myxomatous disease, can lead to altered MV function and cause mitral regurgitation.

1.2. Main Clinical Issues and Current and New Treatment Techniques

Heart valve disease is a significant cause of morbidity and mortality. In the United States, heart valve disease is responsible for about 22,000 deaths per year. In the past two decades, major advances have been made in diagnostic methods in interventional cardiology as well as surgical procedures that have enhanced our understanding of the natural history of valvular heart disease and, thus, have increased patient survival. However, the overall in-hospital mortality rate due to valve procedures is 4.22%, a figure that is much higher than that of other cardiac procedures (24).

The two most common presentations of valve disease are aortic stenosis (AS) and mitral regurgitation (MR). AS is the abnormal narrowing of the AV, which partially obstructs the outflow of blood from the left ventricle (LV). Although currently there is no effective medical therapy for severe AS, surgical aortic valve replacement (AVR) is the definitive therapy and yields low operative mortality for these patients in the absence of serious coexisting conditions. However, in clinical practice, at least 30% of patients with severe symptomatic AS do not undergo AVR surgery, owing to advanced age and the presence of other comorbidities (25). Recently, TAV implantation has emerged as a new treatment for AS in which a bioprosthetic valve is implanted via catheter within the diseased AV. Since the first in-human implantation by Cribier and colleagues (26) in 2002, there has been explosive growth in its use throughout the world. To date, more than 50,000 TAVs have been implanted across 40 countries. The results of several large multicenter registries and the prospective, randomized Placement of Aortic Transcatheter Valves (PARTNER) trial (27) have confirmed this treatment as an alternative to the standard surgical AVR for inoperable and high-risk patients. Initial attempts at TAV implantation in moderate-risk patients are ongoing.

MR is an abnormal leakage of blood from the LV back into the left atrium during systole. The current treatments for MV diseases are surgical repair and replacement of the MV. MV repair, benefiting from improved understanding of MV mechanics and function, is now preferred to valve replacement. Common MV repair techniques include triangular or quadrangular resection, slide annuloplasty, ring annuloplasty, chordal cutting and transposition (28), artificial chord use (29), and, more recently, minimally invasive transcatheter technologies (30). The complex physiology and three-dimensional (3D)

anatomy of the MV and its surrounding structure present substantial challenges when performing these procedures.

1.3. Noninvasive Imaging Modalities for Cardiac Valve Disease Diagnosis

Much of the recent advancement in valvular heart disease evaluation and treatment can be attributed to the advent of noninvasive cardiac imaging modalities, such as echocardiography (Echo), magnetic resonance imaging (MRI), and computed tomography (CT), which are now being used extensively for diagnostics and risk evaluation. Clinicians rely heavily on Echo for evaluating AV and MV morphology. In particular, transesophageal echocardiography (TEE) is commonly used for the evaluation and diagnosis of MV pathology as well as the feasibility of repair. The two-dimensional (2D) TEE provides high-quality images of the MV, yet sometimes the site and degree of prolapse can be incorrectly identified from 2D images (31–33). Consequently, 3D TEE is being increasingly adopted. However, as TEE has a relatively poor spatial resolution compared with MRI and CT, MRI is preferred for analyzing valvular flow characteristics. Because CT has been shown to facilitate more accurate and reproducible AV annular measurements than Echo (34), it is more appropriate for geometric measurement applications, particularly for TAV intervention, for which AV geometries are of importance. Although CT is more readily available and easier to use than cardiac MRI, it comes with the patient risk of radiation exposure.

1.4. Computational Modeling Methods

Most of the imaging modalities offer 3D volumetric, time-resolved data that encompass comprehensive structural and fluid-flow information. Such 3D data, though largely unexploited in clinical settings, offer researchers the possibility to reconstruct the 3D geometry of heart valves at a patient-specific level. When these data are integrated with computational models, native heart valve biomechanical function can be investigated, and preoperative planning tools can be developed for a specific patient. Structural finite element analysis (FEA) can provide a full and detailed quantitative stress and strain analysis of regions of interest, and computational fluid dynamics (CFD) can provide a quantitative description of the flow characteristics. Fully coupled fluid–structure interaction (FSI) methods are also emerging to more comprehensively model valvular biomechanics. However, the accuracy of computational simulations depends heavily on valve geometry, material properties, and the loading and boundary conditions used. Despite the complexity of the AV and MV, most of the early valve models utilized idealized, symmetric geometries of the valve structures and adopted linear elastic material properties. Only in the past several years have clinical images been used to develop patient-specific valve models with improved accuracy. In this review, we outline the advances in valve geometry reconstruction, tissue property modeling, and loading and boundary condition definitions for the purpose of computational structural analysis (i.e., FEA and FSI) of the cardiac valves. The reader is referred to the reviews by Sacks & Yoganathan (35) and Sacks et al. (36) for a more complete overview of the valve biomechanics and to Chandran (37) and Votta et al. (38) for reviews of valve computational studies, particularly CFD studies.

2. MODELING OF VALVE GEOMETRY AND DYNAMIC MOTION

2.1. Ex Vivo Geometry Measurements

Different measurement techniques, including measurements of excised hearts, and silicone rubber casts of the valve and of a functioning valve in vivo have been used to discern the geometry of the AV in several mammalian species. Although the three leaflets often differ in size, they are similar enough to permit a general description of a valve with trileaflet symmetry. The idealization work by Swanson & Clark (39) and Thubrikar (1) allows the geometry of the valve leaflet, root, and sinus to be described by a relatively small set of parameters. This method was adopted by Howard et al. (40) and Labrosse et al. (41, 42), among others, for AV simulations. As shown in Figure 2, representative values of these parameters for an adult human AV are D_b = 26 mm, D_c = 24 mm, H = 16.8 mm, H_s = 6 mm, L_f = 30 mm, L_h = 17 mm, X_s = 3 mm, α = 19°, and β = 7° (43).

Owing to the complex structure of the MV apparatus, early MV modeling efforts also relied on ex vivo dimensional measurements to create finite element (FE) models. For example, Kunzelman et al. (44) measured the annulus lengths, leaflet edge length and height, and anterolateral and posteromedial commissural heights, as well as chordal length and distribution of porcine and human MVs. It should be noted, however, that all measurements were considered planar 2D values. To create 3D models, researchers will need to determine the spatial locations of each of the mitral components. Furthermore, geometric changes to the annulus shape and the papillary muscle locations during the cardiac cycle cannot be captured using ex vivo hearts. Despite these limitations, such geometric modeling methods have been utilized in numerous FE studies of normal (45–48) and pathological (17, 49) MV function. For the purpose of preoperative planning, valve geometries measured ex vivo will not be sufficient.

2.2. Valve Imaging Processing and Valve Segmentation

The precise patient-specific geometry and location of AV and MV features are of critical importance for the proper diagnosis and treatment of valvular diseases. Recently, several research groups have obtained in vivo AV and MV geometries using Echo (50–53), MRI (54–56), and multislice CT scans (19, 57–60) to reconstruct patient-specific AV and MV models. From these images, it is often difficult to identify the more delicate valvular substructures such as the leaflet free edge and chordae tendineae. A more accurate description of the valve structures is achievable, but methods successfully capturing such detail often employ manual tracing or manual geometrical reconstruction by point selection and interpolation (50). For instance, Sirois et al. (59) reconstructed the 3D aortic root and ascending aorta geometries using a custom-made code, vtkPointPicker. Using the software, they manually digitized the 3D locations of aortic root landmarks and output them as a 3D point cloud. They then imported the point cloud into HyperMesh (Altair Engineering, Troy, MI), and generated smooth contour lines of the valve surface to generate FE meshes of the aortic root (59). Figure 3 illustrates the successfully reconstructed 3D valve geometries at 20%, 40%, and 80% of the cardiac cycle that were obtained from the corresponding CT scans. Now, many groups are using semiautomatic methods to segment the valve structures from clinical images through standard image processing techniques, such as intensity-based

thresholding, to distinguish the valve structures from the surrounding blood pool (54, 58, 60, 61). The latest segmentation algorithms being developed can also better segment the valvular structures utilizing data from Echo (62–65), which is preferred to CT in the clinical setting. Still, the efficient transfer of volumetric imaging data into FEA remains a challenge.

Recent efforts in clinical image processing have been focused on improving efficiency for real-time use (31, 63, 66). Automated methods are based on deformable template geometries of the valve structures and the probabilities of the shape variation modes. Mahmood et al. (31) intraoperatively reconstructed a model of the MV geometry derived from 3D TEE data using the Mitral Valve Analysis Package (TomTec Imaging Systems GmbH, Munich, Germany). The authors first delineated the mitral leaflets by the anterior, posterior, anterolateral, and pos-teromedial landmarks. They then identified the MA on 2D cuts through the landmark points. Ionasec et al. (66) presented an automatic system for the simultaneous segmentation and landmark detection of the AV and MV from CT and TEE imaging data. Pouch et al. (62) have also presented a consistent automatic segmentation and shape reconstruction method for the AV from 3D Echo images. For the purpose of optimizing TAV implantation, Zheng et al. (63) have developed a part-based automatic aorta segmentation approach for C-arm CT data. The part-based model facilitates the independent recognition and segmentation of the entire aorta including the arch and the ascending and descending sections. The algorithm can process the aorta volume in 1.1 s and could help cardiologists determine the proper TAV angulation during deployment (63).

2.3. Subject-Specific Dynamic Model

Many of the segmentation methods discussed above are static or single-moment snapshots. The segmentation process would have to be repeated for additional time points in order to analyze the dynamic valve geometries through the cardiac cycle. Real-time visualization of the 3D valve geometries throughout function could also greatly benefit clinicians. There are now two dynamic valve models in the literature to address this need. Veronesi et al. (67) were among the first groups to quantify the 3D AV and MV dynamics from matrix-array transesophageal images. The AV and MV features were semiautomatically detected and then automatically tracked through the cardiac cycle. Ionasec et al. (66) have also developed a dynamic model of the AV and MV with the ability to capture morphologic and pathologic differences over an entire cardiac cycle based on the trajectories of landmark points. The robustness and accuracy of the method were demonstrated by extensive experiments on 1,516 TEE and 690 cardiac CT volumes with an average processing time of 4.8 s and an average accuracy within 1.45 mm of the expert-defined ground truth. The use of subject-specific dynamic valve models for preoperative planning holds great promise; however, an automated, fast, and user-friendly method to load 3D imaging data, refine them into nonlinear FE models, and then further visualize and process simulations with them has not yet been developed.

3. CHARACTERIZATION OF MATERIAL PROPERTIES OF VALVE TISSUES

3.1. Animal and Human Valve Tissue Properties

Owing to the limited availability of human tissues, our current knowledge of valve tissue mechanical properties is derived mainly from work with porcine or ovine valves (2, 68–78). There are numerous studies in the literature that use animal valve tissues as surrogates for human tissues (2, 15, 76–79). Lo & Vesely (76) were among the first to characterize the biaxial properties of porcine AV leaflets. Representative works also include Billiar & Sacks (77), Stella & Sacks (2), and Stephens & Grande-Allen (78), which have quantified the biaxial properties of porcine AV leaflets under multiloading protocols, as well as layer-specific and age-dependent conditions. Recently, Martin & Sun (16) reported the first data set of biaxial properties of aged human and ovine AV leaflets. Human aortic tissue material properties have recently been incorporated in the TAV simulation studies by Wang et al. (58) and Auricchio et al. (80). On the MV side, May-Newman & Yin (68) and Kunzelman & Cochran (69) pioneered the studies on the planar biaxial mechanical response of porcine MV leaflets. Their experimental data sets have been used extensively in constitutive material modeling (45, 81) and simulation of MV dynamics at physiological conditions (55, 61, 82–84). Several groups have also investigated animal MV biomechanics through in vivo experiments (73, 82, 85–86), although there is a lack of such studies for the human MV. The few studies on the mechanical properties of the human MV are ex vivo studies. Clark (87) and Prot et al. (18) measured the uniaxial response of the MV leaflets, and Pham & Sun (88) conducted biaxial mechanical tests of the MV leaflets from 21 aged human hearts. Properties of the human MV were recently applied in the FE simulation of MV function by Wang & Sun (19).

Experimental studies have demonstrated significant differences between the mechanical properties of animal and aged human tissues, including the aortic root (14), AV (16), coronary sinus (89), and MV (88). In all cases, the aged human tissues were much stiffer, as shown in Figure 4. Because the aged population is the key demographic for valvular disease, the use of animal tissue properties for simulations related to valvular repair or replacement may compromise the validity of the results. The future use of these animal models in evaluating valve device mechanical function must be considered with caution (90).

3.2. Constitutive Models of Valve Tissues

3.2.1. Linear elastic models—Early attempts to describe valve tissue properties relied on the linear elastic material model, following the generalized Hooke's law (8, 45)

$$\sigma_{ij}=C_{ijkl}\varepsilon_{kl}, \quad (1)$$

where σ_{ij} is the stress tensor, ε_{kl} is the strain tensor, and C_{ijkl} is the fourth-order elasticity tensor. Linear elastic models are appropriate when the stress–strain relationship is indeed linear, and are typically restricted to relatively small deformations. Linear elastic material properties were chosen for various reasons (55, 61, 91), but mainly to simplify the simulation process in order to achieve numerical convergence in FE simulation solutions.

Over the physiological range of pressures, valve tissues have been shown to exhibit a relatively linear stress–strain relationship (86). However, for a FE simulation of valve deformation from the undeformed state to a deformed state, the valve material response is clearly nonlinear, and the use of nonlinear material models is essential for realistic valve simulations.

3.2.2. Fung-elastic model—The Green strain–based exponential model proposed by Fung (92) is probably the most commonly used hyperelastic model for characterizing the mechanical response of soft tissues (92, 93). A two-dimensional Fung-type strain energy function W can be expressed as

$$W=\frac{c}{2}[e^{Q}-1], \quad (2)$$

$$Q=A_1E_{11}^2+A_2E_{22}^2+2A_3E_{11}E_{22}+A_4E_{12}^2+2A_5E_{11}E_{22}+2A_6E_{22}E_{12}, \quad (3)$$

where c and A_i are material constants, and $\boldsymbol{E}$ is the Green strain tensor. Note that Equation 2 has other variants that could easily be treated as a subset or expansion of this model (94). Equation 2 is often used to model planar biaxial mechanical responses of valve tissues (95) and should be implemented with plane stress elements, such as shell or membrane elements. One problem with Equation 2 is that the transverse shear stiffness (TSS) in the 13 and 23 directions are undetermined owing to the lack of transmural response definitions in this model. As shown by Sun et al. (94), the valve peak stress is insensitive to changes in TSS values for the valve closure simulation. However, to simulate valve opening, the tissue bending response is critical, and without accurate TSS values, Equation 2 may give inaccurate results. Additional details on FE implementation of Equation 2 can be found in Sun & Sacks (96). The 3D Fung model has not been widely used to model valve functions; however, Labrosse and colleagues (41, 42) successfully utilized a 3D Fung model to simulate native AV deformation.

3.2.3. Strain invariant–based fiber-reinforced hyperelastic model—Weiss et al. (97) and Holzapfel et al. (98) presented a computational framework to implement strain invariant–based models that can accommodate the effects of one or two families of elastic fibers. To use this class of models, typically, the valve tissues are assumed to be composed of a matrix material with two families of embedded fibers, each with a preferred direction. The deviatoric strain invariant $\overline{I_1}$ is used to describe the matrix material, and $\overline{I_{4i}}$ is used to describe the properties of the fiber families. One example of such models proposed by Holzapfel et al. (98) can be expressed as

$$W=C_{10}\left(\overline{\mathrm{I}_1}-3\right)+\frac{k_1}{2k_2}\sum_{i=1}^{2}\left[\exp\left\{k_2\left[\kappa\overline{\mathrm{I}_1}+(1-3\kappa)\overline{\mathrm{I}_{4\mathrm{i}}}-1\right]^2\right\}-1\right]+\frac{1}{D}(J-1)^2,\ i=1,2, \quad (4)$$

where C_{10}, k_1, k_2, and D are material constants. Specifically, C_{10} describes the matrix material, and D enforces near incompressibility. In addition, a dispersion parameter, κ, is used to describe the distribution of the fiber orientation. Local coordinate systems should be defined for each leaflet to include fiber orientations. There are several variations of the model that have been applied to heart valve simulations. Prot et al. (18) implemented the Holzapfel material model in the analysis of healthy and pathological human MVs. Wang and colleagues (19, 58) simulated AV and MV functions with a variation of the material model. Similarly, Stevanella et al. (55) simulated the MV dynamics and characterized leaflet properties through a transversely isotropic model proposed by May-Newman & Yin (99), while Conti et al. (100) and Auricchio et al. (80) used the same material model to simulate AV biomechanics.

4. DEFINITION OF LOADING AND BOUNDARY CONDITIONS

For the FE quasi-static simulation of AV closure, a uniform pressure field, typically with a maximum of 120 mm Hg, is applied on the aortic side of the leaflets. This approach is frequently used and sufficient to obtain the valve stress distribution. However, one should consider these results with caution: The dynamic loading due to the blood flow–induced dynamic “water hammer” effect is ignored in any quasi-static valve simulation. For FE simulation of AV opening, a static transvalvular pressure of 4–7 mm Hg may be applied on the ventricular side of the leaflets to open the valve. In such simulations, the valve free edge may be overly expanded because the actual transvalvular pressure at the free edge should be close to 1–2 mm Hg when the valve is fully open. Thus, the effective orifice area calculation from FE static simulation results may not be accurate. For FE dynamic simulation, the time-dependent pressures on the corresponding sides of the leaflets can be applied. However, owing to the lack of blood viscosity damping on the leaflets, the leaflet motion may exhibit excessive, unrealistic vibrations. In the case of FSI analysis, pressure on the leaflets is a consequence of the fluid dynamics; thus, the loading condition is more realistically modeled.

For the MV, owing to the complicated contact between the leaflets, dynamic explicit analysis is usually conducted to simulate the valve closing process. To mimic the mitral annular and papillary muscle dynamics due to the contraction of the surrounding LV, nodal displacements of the MA and chordal origins on the papillary muscles can be tracked from clinical images, such as CT scans (19), at different phases during the cardiac cycle. A time-dependent physiological transmitral pressure of one cardiac cycle can be applied on the ventricular side of the mitral anterior and posterior leaflets. Similar to AV simulations, modeling of valve FSI is needed to capture the realistic loading conditions of the MV. Additionally, LV and papillary muscles with active contraction should be incorporated to accurately simulate the dynamic boundary conditions of the MV.

5. COMPUTATIONAL SIMULATION OF CARDIAC VALVE FUNCTION AND INTERVENTION

5.1. Aortic Valve Applications

Early studies employing FEA to investigate human AV function began in the 1970s (8, 101, 102). Valve leaflet geometry data were obtained from photogrammetric analysis of molds made from human AVs, and thin-shell FE models were generated to perform linear elastic stress analysis (8). The goal of these and other early computational AV studies was mainly to understand basic valve functions under both physiological and pathological conditions. To this end, simplified models can still offer a wealth of knowledge. For instance, researchers have found that the bicuspid aortic valve (BAV) geometry results in increased leaflet stresses and strains (3, 4, 6) and reduced valve effective orifice area (EOA) (3), which may explain the greater tendency of these patients to develop AS, as well as aortic aneurysm and dissection, compared with patients with a normal tricuspid AV. Grande-Allen and colleagues have also applied FE models to study the effects of valvular insufficiency (7) and Marfan syndrome (9) and concluded that both pathologies tend to increase leaflet stresses and strains. Although informative for parametric studies, these studies are somewhat limited by numerical assumptions such as linear elastic tissue properties (7–9, 102), animal-derived tissue properties (4, 6), or idealized geometry (6, 8, 102).

Because the preferred method of treatment for AV disease is surgical replacement of the diseased valve with a prosthetic, many computational studies have focused on prosthetic valve function and design. Computational studies have shown that by changing bioprosthetic valve design, through varying manufacturing techniques (103), leaflet shapes (104), and frame mounting methods (103, 105–108), the stress distribution pattern acting on the leaflets can be altered. There are relatively few studies of surgical AV repairs, which are associated mainly with the Yacoub/David valve-sparing techniques (109). Labrosse et al. (41) have simulated leaflet correction techniques, such as central and commissural plication and resuspension of the leaflet free margin. They found that leaflet resuspension appeared to be the best among the three techniques. Grande-Allen et al. (10) studied the influence of aortic graft shape and stiffness in the valve-sparing procedure and showed that although commercial vascular grafts are made of polyethylene terephthalate, a graft made of polycarbonate urethane could replicate the native valve biomechanics more closely. Other studies also applied FE simulation to study AV-sparing via grafting and showed that different procedures (110), as well as differently sized (111) and shaped (112, 113) vessel grafts, could have a significant impact.

FEA combined with patient-specific imaging data could potentially be utilized as a tool to refine patient selection, evaluate device performance, and eventually improve clinical outcomes for individual patients. Several FE models (58, 60, 80) have been developed to analyze the biomechanics involved with TAV implantation in specific patients. Auricchio et al. (80) simulated both Edwards SAPIEN stent crimping and deployment through balloon inflation in a patient-specific aortic root model. From the simulation they were able to determine the effect of device positioning on the leaflet and aortic wall stresses. Wang et al. (58) developed a patient-specific FE model to quantify the biomechanical interaction

between the TAV stent and the stenotic AV. This analysis included modeling of the native aortic leaflets, ascending aorta, and surrounding myocardium, which were defined by biaxial testing data of human aortic tissues (14, 16). From the simulation results, Wang et al. (58) showed that calcium deposits on the leaflets may inhibit stent expansion and ultimately result in paravalvular leak.

The inherent limitation of all purely structural analyses for the AV is the lack of blood interaction. De Hart et al. (11) developed the first 3D AV FSI model using the Lagrange multiplier–based fictitious domain method to study the kinematic opening and closing behavior of the valve. This study marked an improvement over most prior structural analyses, which dealt only with valve closing (11). Nicosia et al. (114) employed a similar method to study the FSI of the AV and root, utilizing a more realistic geometry extracted from MRI data. Through FSI studies, Katayama et al. (5) discovered that the sinuses facilitate smooth closure of the AV and reduce stress concentrations in the leaflets, and Marom et al. (12) demonstrated significant discrepancies in simulated AV leaflet coaptation area, contact pressure, and valve closing time when compared with purely structural analyses of AV closing. However, the complex nature of the leaflet fluid–structure interaction has hindered progress in this area. Each of these FSI analyses include significant assumptions, including idealized geometries, unrealistic leaflet material, and simplified fluid flow properties. Only the most recent FSI models have included more sophisticated material models. For instance, the most recent FSI model by Marom et al. (115) includes the asymmetric collagen fiber architecture of a porcine valve built into the leaflet material, and a compliant root. They found that the asymmetric fiber architecture alters the valve kinematics and flow characteristics (115). Katayama and colleagues have also utilized an anisotropic, albeit linear, leaflet property. Still, significant progress must be made in order to develop accurate patient-specific FSI models of the AV.

5.2. Mitral Valve Applications

Kunzelman and coworkers were among the pioneers in developing 3D FE models of the normal (45) and pathologically altered (49, 116) MV. Their MV model, albeit limited by symmetric geometry based on the excised porcine MV, included all the essential components of an MV. The model has been used extensively to analyze various MV repair procedures (116–118). Although various designs of annuloplasty rings, including undersized, rigid, semirigid, flexible, D-shape, and dog-bone shaped, are commercially produced, the optimal shape is uncertain. Kunzelman et al. (116) developed static FE models of the normal and dilated MV to simulate the effects of flexible and rigid annuloplasty rings. Subsequently, Maisano et al. (119) and Votta et al. (91) showed that the dog bone–shaped annuloplasty ring with selective reduction in the septolateral dimension is more effective than a conventional prosthesis for treating leaflet tethering in functional MR. However, these studies excluded or simplified the LV geometry. Wong et al. (120) reconstructed a 3D FE model incorporating the LV, annulus, and chordae tendineae from 3D cardiac MRI images of sheep. They successfully simulated the MR scenario and observed that the stress reduction with the saddle-shaped MA was slightly greater than that of the asymmetric rings. More recently, research groups have begun to construct in vivo patient-specific MV models using clinical Echo (50, 121) and MRI (54, 55). For instance, 3D Echo images were used by Xu et al.

(121) to reconstruct MV models to predict leaflet and chordal stresses. MV geometries were perturbed to examine how MV leaflet coaptation area, noncoapted leaflet area, and interleaflet coefficient of friction affect leaflet and chordal stress distribution. The results indicated that MV repair techniques that increase or preserve noncoapted leaflet area might decrease stresses and thereby enhance repair durability. Similarly, Stevanella et al. (55) utilized cardiac MRI to develop patient-specific MV models of one healthy subject and one patient with ischemic MR. Their disease model captured actual regurgitant characteristics and revealed abnormal tensions in the annular region and subvalvular apparatus.

One of the inaccuracies in MV modeling is the bulging of anterior leaflet into the atrium, which could be due to incorrect assumptions about chordal length, chordal origins, and insertion points at the mitral leaflets. Such structure details are not distinguishable in the current clinical MRI or TEE images owing to their poor spatial resolution. Multislice CT images offer much better spatial resolution (e.g., 64-slice CT of 0.625 mm). CT images were used by Wang & Sun (19) to reconstruct patient-specific MV models. In their study, the MV models incorporated not only the mitral leaflet thickness but also the papillary muscle locations, chordal origins, and chordal insertion points, as shown in Figure 5. Dynamic motions of the MA and papillary muscles were obtained from middle systole and middle diastole and were prescribed as boundary conditions for the FE simulation. Simulation results were validated by comparing FE-deformed MV geometries with the CT images at systole, and a close match was obtained (Figure 5*c*) (19). Significant bulging of the mitral leaflets was not observed at peak transmitral pressure (19). As there is evidence of muscle fibers and innervation in mitral leaflets (122), Skallerud et al. (123) applied a simple active stress component in modeling the porcine MV, which resulted in a significant reduction in the leaflet bulging.

Percutaneous catheter-based edge-to-edge (ETE) mitral repair using MitraClip has grown rapidly in Europe during the past few years. Over 10,000 MitraClips have been implanted worldwide to date (124). MV mechanics under ETE conditions are thus of great interest. Using idealized geometries of the MV and LV, Radaelli et al. (125) and Fiore et al. (126) were able to provide a good estimation of the pressure drop across the ETE-repaired valve and assess the leaflet stress pattern from the 8-mm ETE suture (127). Consistent with clinical observations, FE simulations confirmed that using an annuloplasty ring in conjunction with ETE repair is favorable if mitral annular dilation is present, as it could reduce leaflet stresses (128, 129). Dal Pan et al. (130) employed a parametric study of the ETE technique to investigate stress and strain distributions on leaflets at various suture positions and extension lengths as well as dilated annulus dimensions. The study provides useful analyses for technique improvement and optimization.

There are relatively few FSI studies on MV structural and hemodynamic function. Kunzelman et al. (17) developed a fully coupled FSI model using LS-DYNA (Livermore Software Technology Corp., Livermore, CA). For this model, they substantially enhanced their previous models (45) by incorporating a fiber-reinforced hyperelastic material model for the leaflets, nonuniform leaflet thickness, branched chords, and fluid flow. The simulation results agreed well with physiological data reported in the literature. By varying the parameters of the fiber model, the authors also investigated effects of pathological

changes. More recently, Ma et al. (131) developed an FSI MV model using the immersed boundary method. The model was generated from MRI data of a healthy patient. Linear elastic material models were used for both leaflets and chords. From the simulation results, the authors concluded that the differences in the thicknesses of the leaflets play an important role in maintaining the physiological curvature of the MV leaflet during its dynamic motion. Neither Kunzelman et al. (17) nor Ma et al. (131) incorporated the left atrium and LV into their models. Dahl et al. (132), however, reported an FSI study on MV behavior during LV filling with the realistic left atrium and LV geometry obtained from Echo. Though limited by stemming from a 2D simulation with prescribed rigid wall motions (thus, not a coupled FSI), their results underscore the importance of incorporating the asymmetric leaflet geometry and left atrium to obtain accurate MV flow fields.

6. FUTURE DIRECTIONS

6.1. Quantification of In Vivo Human Tissue Properties

Although the use of age-matched human tissue properties in valve simulations is a substantial improvement over use of animal tissue properties, there are also limitations to using ex vivo tissue properties from human cadaveric hearts. First of all, ex vivo tissue properties are not patient specific. Rather the tissue properties are selected from a cadaveric heart with similar characteristics (age, sex, etc.) to the patient of interest. This requires a thorough testing database of human tissue properties from an array of patients with differing ages (133), genders, and degrees of disease because all these factors can significantly impact cardiovascular tissue properties. Furthermore, tissue property homogeneity is generally assumed over a particular region. Ex vivo testing data generally represent only the average response from the center region of a specimen. In reality, the tissue structure and the associated mechanical properties are heterogeneous. The ultimate goal would be to obtain the patient-specific tissue properties from noninvasive imaging modalities using either the inverse FE method or new techniques. It is possible to measure aortic tissue expansion over the cardiac cycle by utilizing time-elapsed noninvasive imaging modalities (133). The difficulty is that the physiological stress/strain range is rather narrow. The challenge that remains is how to quantify the arterial material responses at low (0–80 mm Hg) and high (>120 mm Hg) stress levels to obtain the complete material response, from the unstressed and unloaded state to the state of tissue dissection, tear, and rupture. Several groups have adopted an inverse FE procedure to perform stress analysis from in vivo imaging (134–136); however, such approaches have not been applied to valve tissues. A future effort could be to develop an inverse FE method that would utilize existing databases of human tissue properties to guide the inverse FE solution progress.

6.2. Patient-Specific and Population-Based Probabilistic Simulation for Valve Intervention

To translate computational modeling techniques to clinical practice, one important future application is to develop a computational patient-specific, preoperative planning system for TAV intervention. Using patient CT imaging data, Wang et al. (137) have developed realistic patient-specific FE models of TAV intervention that incorporate human aortic tissue material properties with material failure criteria built in. The TAV deployment and tissue-device interaction were simulated in five case studies, including one annular rupture case, three

successful cases, and one successful valve-in-valve case. In the rupture case of a 94-year-old female with an annulus measuring 19.6 mm, the CT scans showed that, owing to heavy calcification, only her left coronary leaflet could open. In the actual TAV procedure, a size 23 Edwards SAPIEN valve was used, and unfortunately, the aortic root tore below the left main coronary artery. Emergency open-heart valve surgery was consequently performed. The case (i.e., images and clinical data) was sent for a biomechanical analysis. FE simulations predicted that the aortic root tearing would occur below the left main coronary artery (Figure 6), which matched clinical observations. These results demonstrate the potential for computational modeling techniques to be incorporated into the preprocedural evaluation process.

Yet, in order for the current computational models to be utilized as a preoperative planning tool for valve intervention in the future, the spatial resolution from clinical images should be further improved. An image spatial resolution of 0.1 mm is likely needed to clearly distinguish valve leaflet free edge and chordal shape, origin, and insertion locations. The computational efficiency of interventional simulations should also be improved for practicality. Although it is not a common clinical practice to perform CT scans after TAV implantation, postprocedural CT imaging would be conducive to thorough validation of the FE models. Validation of the models should be completed over a large number of TAV implantation cases to assure the accuracy of the model development methodology.

Whereas patient-specific analyses are essential for accurate preoperative planning, population-based probabilistic studies will be pivotal in the design of reliable valve prostheses and implantation techniques. Human anatomic valve geometries and their associated tissue properties are highly variable. The design of valve devices should be robust to account for the uncertainty of these variables and to avoid adverse clinical events and clarify patient selection criteria. Probabilistic computational analysis permits a rigorous quantification of various uncertainties and has been successfully applied to the design and analysis of a variety of engineering systems, including space vehicles and automobiles (138) and, more recently, orthopedic implants (139–142). A probabilistic valve model should be built from a deterministic computational model, as described in Section 5, with additional steps to include probabilistic analysis. The additional steps are (*a*) definition of random variable inputs, (*b*) mapping of random variables to the model, (*c*) selection of responses from the model, and (*d*) probabilistic analysis and interpretation of results. Such an approach has recently been applied by Li & Sun (143) for probabilistic analysis of TAV leaflet design.

6.3. Multiscale Computational Analysis

A normal heart valve functions at multiple length scales, including organ, tissue, cellular, and molecular scales (144). As the overall behavior of the heart valve is linked to every length scale, alteration of one scale would trigger and activate changes in another. Therefore, one cannot fully describe the heart valve biomechanics from a single length scale. Mechanical stimuli, such as transvalvular pressures, impose stretches on the organ scale that translate to the tissue scale (36). It has been shown that such dynamic deformation in vitro can mediate the responses of valvular interstitial cells (VICs), which serve to maintain tissue structural integrity via protein synthesis and enzymatic degradation. Huang et al. (145)

quantified the aortic VIC deformation under a quasi-static physiological pressure. They found that the nuclear aspect ratios, measured as an index of overall cellular strain, increased substantially from 4 to 90 mm Hg, with the fibrosa layer exhibiting a greater rate of change compared with the ventricular layer. Owing to the heterogeneity of the leaflet structure, Vesely & Noseworthy (146) studied the layer-specific mechanical properties of the porcine AV leaflet. By separating the fibrosa and the ventricularis from fresh and glutaraldehyde-fixed porcine aortic leaflets, they found that although the two layers differ structurally, they complement each other mechanically during AV function (e.g., more radial extensibility to facilitate valve closure). Later, Stella & Sacks (2) characterized the material properties of the layers using strip biaxial tests. Their mechanical data were later implemented in a series of computational studies by Weinberg & Mofrad (147), who developed a computational model to simulate the mechanical behaviors of valves across the range of length scales. In their most recent study, Weinberg and coworkers (148) performed a multiscale simulation in both solid and fluid domains to analyze whether the geometric difference or the mechanical deformation difference causes the major differences in function and pathology (e.g., calcification) between normal tricuspid valves and BAVs. Interestingly, their model predicted that cellular-scale deformations are similar in both valves regardless of organ-scale differences, suggesting calcification may instead be due to a genetic difference that gives rise to a difference in matrix constituents. Limitations of the study that may have affected their results include modeling both tissue and cellular scales using isotropic constitutive relations, the use of homogenized BAV tissue structures, and the lack of BAV tissue properties. Although their cellular-scale model was greatly simplified, their simulation was the first to link across the length scales to create a multiscale model. Clearly, much more computational work remains to be done at cellular and molecular levels, and innovative methods linking both the spatial and temporal scales to simulate the development of pathological events have yet to be developed.

7. CONCLUSION

Heart valve disease, most commonly presenting as aortic stenosis or mitral regurgitation, is a significant cause of morbidity and mortality. Recent advances in computational modeling of the cardiac valves, including enhanced noninvasive imaging, innovative 3D anatomic geometry reconstruction methods, and improved structural modeling and simulation techniques, have enabled realistic simulation of valve biomechanics. Although significant work to validate the predictability of such simulations still remains to be done, further development in these areas will pave the way for exciting new avenues, such as patient-specific, preoperative planning and probabilistic, population-based evaluation of valve devices and treatment methods.

Glossary

STJ	sinotubular junction
TAV	transcatheter aortic valve
SOV	sinuses of Valsalva

MV	mitral valve
MA	mitral annulus
AML	anterior mitral leaflet
PML	posterior mitral leaflet
AS	aortic stenosis
MR	mitral regurgitation
LV	left ventricle
AVR	aortic valve replacement
Echo	echocardiography
MRI	magnetic resonance imaging
CT	computed tomography
TEE	transesophageal echocardiography
FEA	finite element analysis
FSI	fluid–structure
BAV	bicuspid aortic
ETE	edge-to-edge (mitral repair)

LITERATURE CITED

1. Thubrikar, M. The Aortic Valve. Boca Raton, FL: CRC; 1990.
2. Stella JA, Sacks MS. On the biaxial mechanical properties of the layers of the aortic valve leaflet. J Biomech Eng. 2007; 129:757–66. [PubMed: 17887902]
3. Jermihov PN, Jia L, Sacks MS, Gorman RC, Gorman JH III, Chandran KB. Effect of geometry on the leaflet stresses in simulated models of congenital bicuspid aortic valves. Cardiovasc Eng Technol. 2011; 2:48–56. [PubMed: 21980326]
4. Conti C, Della Corte A, Votta E, Del Viscovo L, Bancone C, et al. Biomechanical implications of the congenital bicuspid aortic valve: a finite element study of aortic root function from in vivo data. J Thorac Cardiovasc Surg. 2010; 140:890–96. [PubMed: 20363481]
5. Katayama S, Umetani N, Sugiura S, Hisada T. The sinus of Valsalva relieves abnormal stress on aortic valve leaflets by facilitating smooth closure. J Thorac Cardiovasc Surg. 2008; 136:1528–35. 1535.e1. [PubMed: 19114202]
6. Katayama S, Umetani N, Hisada T, Sugiura S. Bicuspid aortic valves undergo excessive strain during opening: a simulation study. J Thorac Cardiovasc Surg. 2013; 145:1570–76. [PubMed: 22698558]
7. Grande KJ, Cochran RP, Reinhall PG, Kunzelman KS. Mechanisms of aortic valve incompetence: finite element modeling of aortic root dilatation. Ann Thorac Surg. 2000; 69:1851–57. [PubMed: 10892936]
8. Cataloglu A, Clark RE, Gould PL. Stress analysis of aortic valve leaflets with smoothed geometrical data. J Biomech. 1977; 10:153–58. [PubMed: 858719]

9. Grande-Allen KJ, Cochran RP, Reinhall PG, Kunzelman KS. Mechanisms of aortic valve incompetence: finite-element modeling of Marfan syndrome. J Thorac Cardiovasc Surg. 2001; 122:946–54. [PubMed: 11689800]
10. Grande-Allen K, Cochran R, Reinhall P, Kunzelman K. Finite-element analysis of aortic valve-sparing: influence of graft shape and stiffness. IEEE Trans Biomed Eng. 2001; 48:647–59. [PubMed: 11396595]
11. De Hart J, Peters GWM, Schreurs PJG, Baaijens FPT. A three-dimensional computational analysis of fluid–structure interaction in the aortic valve. J Biomech. 2003; 36:103–12. [PubMed: 12485644]
12. Marom G, Haj-Ali R, Raanani E, Schafers H-J, Rosenfeld M. A fluid–structure interaction model of the aortic valve with coaptation and compliant aortic root. Med Biol Eng Comput. 2012; 50:173–82. [PubMed: 22170305]
13. Chandra S, Rajamannan N, Sucosky P. Computational assessment of bicuspid aortic valve wall-shear stress: implications for calcific aortic valve disease. Biomech Model Mechanobiol. 2012; 11:1085–96. [PubMed: 22294208]
14. Martin C, Pham T, Sun W. Significant differences in the material properties between aged human and porcine aortic tissues. Eur J Cardiothorac Surg. 2011; 40:28–34. [PubMed: 21177118]
15. Gundiah N, Matthews PB, Karimi R, Azadani A, Guccione J, et al. Significant material property differences between the porcine ascending aorta and aortic sinuses. J Heart Valve Dis. 2008; 17:606–13. [PubMed: 19137790]
16. Martin C, Sun W. Biomechanical characterization of aortic valve tissue in humans and common animal models. J Biomed Mater Res Part A. 2012; 100A:1591–99.
17. Kunzelman KS, Einstein DR, Cochran RP. Fluid–structure interaction models of the mitral valve: function in normal and pathological states. Philos Trans R Soc B Biol Sci. 2007; 362:1393–406.
18. Prot V, Skallerud B, Sommer G, Holzapfel GA. On modelling and analysis of healthy and pathological human mitral valves: two case studies. J Mech Behav Biomed Mater. 2010; 3:167–77. [PubMed: 20129416]
19. Wang Q, Sun W. Finite element modeling of mitral valve dynamic deformation using patient-specific multi-slices computed tomography scans. Ann Biomed Eng. 2013; 41:142–53. [PubMed: 22805982]
20. Lam JH, Ranganathan N, Wigle ED, Silver MD. Morphology of the human mitral valve. I Chordae tendineae: a new classification. Circulation. 1970; 41:449–58. [PubMed: 5415982]
21. Timek TA, Green GR, Tibayan FA, Lai DT, Rodriguez F, et al. Aorto-mitral annular dynamics. Ann Thorac Surg. 2003; 76:1944–50. [PubMed: 14667619]
22. Marzilli M, Sabbah HN, Lee T, Stein PD. Role of the papillary muscle in opening and closure of the mitral valve. Am J Physiol. 1980; 238:H348–54. [PubMed: 7369379]
23. Madu EC, D'Cruz IA. The vital role of papillary muscles in mitral and ventricular function: echocardiographic insights. Clin Cardiol. 1997; 20:93–98. [PubMed: 9034636]
24. Lloyd-Jones D, Adams RJ, Brown TM, Carnethon M, Dai S. Heart disease and stroke statistics—2010 update: a report from the American Heart Association. Circulation. 2010; 121:e46–215. [PubMed: 20019324]
25. Webb JG, Wood DA. Current status of transcatheter aortic valve replacement. J Am Coll Cardiol. 2012; 60:483–92. [PubMed: 22749306]
26. Cribier A, Eltchaninoff H, Bash A, Borenstein N, Tron C, et al. Percutaneous transcatheter implantation of an aortic valve prosthesis for calcific aortic stenosis: first human case description. Circulation. 2002; 106:3006–8. [PubMed: 12473543]
27. Leon MB, Smith CR, Mack M, Miller DC, Moses JW, et al. Transcatheter aortic-valve implantation for aortic stenosis in patients who cannot undergo surgery. N Engl J Med. 2010; 363:1597–607. [PubMed: 20961243]
28. Carpentier A. Cardiac valve surgery—the "French correction. J Thorac Cardiovasc Surg. 1983; 86:323–37. [PubMed: 6887954]
29. Privitera S, Butany J, Silversides C, Leask RL, David TE. Artificial chordae tendinae: long-term changes. J Card Surg. 2005; 20:90–92. [PubMed: 15673420]

30. Feldman T, Foster E, Glower DG, Kar S, Rinaldi MJ, et al. Percutaneous repair or surgery for mitral regurgitation. N Engl J Med. 2011; 364:1395–406. [PubMed: 21463154]
31. Mahmood F, Karthik S, Subramaniam B, Panzica PJ, Mitchell J, et al. Intraoperative application of geometric three-dimensional mitral valve assessment package: a feasibility study. J Cardiothorac Vasc Anesth. 2008; 22:292–98. [PubMed: 18375338]
32. Chauvel C, Bogino E, Clerc P, Fernandez G, Vernhet JC, et al. Usefulness of three-dimensional echocardiography for the evaluation of mitral valve prolapse: an intraoperative study. J Heart Valve Dis. 2000; 9:341–49. [PubMed: 10888088]
33. Ahmed S, Nanda NC, Miller AP. Usefulness of transesophageal three-dimensional echocardiography in the identification of individual segment/scallop prolapse of the mitral valve. Echocardiography. 2003; 20:203–9. [PubMed: 12848691]
34. Jabbour A, Barker S, Davies S, Prasad SK, Rubens M, Mohiaddin RH. Multimodality imaging in transcatheter aortic valve implantation and post-procedural aortic regurgitation: comparison among cardiovascular magnetic resonance, cardiac computed tomography, and echocardiography. J Am Coll Cardiol. 2011; 58:2165–73. [PubMed: 22078422]
35. Sacks MS, Yoganathan AP. Heart valve function: a biomechanical perspective. Philos Trans R Soc B Biol Sci. 2007; 362:1369–91.
36. Sacks MS, Merryman WD, Schmidt DE. On the biomechanics of heart valve function. J Biomech. 2009; 42:1804–24. [PubMed: 19540499]
37. Chandran KB. Role of computational simulations in heart valve dynamics and design of valvular prostheses. Cardiovasc Eng Technol. 2010; 1:18–38. [PubMed: 20606715]
38. Votta E, Le TB, Stevanella M, Fusini L, Caiani EG, et al. Toward patient-specific simulations of cardiac valves: state-of-the-art and future directions. J Biomech. 2013; 46:217–28. [PubMed: 23174421]
39. Swanson M, Clark RE. Dimensions and geometric relationships of the human aortic valve as a function of pressure. Circ Res. 1974; 35:871–82. [PubMed: 4471354]
40. Howard IC, Patterson EA, Yoxall A. On the opening mechanism of the aortic valve: some observations from simulations. J Med Eng Technol. 2003; 27:259–66. [PubMed: 14602517]
41. Labrosse MR, Boodhwani M, Sohmer B, Beller CJ. Modeling leaflet correction techniques in aortic valve repair: a finite element study. J Biomech. 2011; 44:2292–98. [PubMed: 21683361]
42. Labrosse MR, Lobo K, Beller CJ. Structural analysis of the natural aortic valve in dynamics: from unpressurized to physiologically loaded. J Biomech. 2010; 43:1916–22. [PubMed: 20378117]
43. Labrosse MR, Beller CJ, Robicsek F, Thubrikar MJ. Geometric modeling of functional trileaflet aortic valves: development and clinical applications. J Biomech. 2006; 39:2665–72. [PubMed: 16199047]
44. Kunzelman KS, Cochran RP, Verrier ED, Eberhart RC. Anatomic basis for mitral valve modelling. J Heart Valve Dis. 1994; 3:491–96. [PubMed: 8000582]
45. Kunzelman KS, Cochran RP, Chuong C, Ring WS, Verrier ED, Eberhart RD. Finite element analysis of the mitral valve. J Heart Valve Dis. 1993; 2:326–40. [PubMed: 8269128]
46. Einstein DR, Kunzelman KS, Reinhall PG, Cochran RP, Nicosia MA. Haemodynamic determinants of the mitral valve closure sound: a finite element study. Med Biol Eng Comput. 2004; 42:832–46. [PubMed: 15587476]
47. Prot V, Skallerud B, Holzapfel GA. Transversely isotropic membrane shells with application to mitral valve mechanics: constitutive modelling and finite element implementation. Int J Numer Methods Eng. 2007; 71:987–1008.
48. Lau KD, Diaz V, Scambler P, Burriesci G. Mitral valve dynamics in structural and fluid–structure interaction models. Med Eng Phys. 2010; 32:1057–64. [PubMed: 20702128]
49. Kunzelman KS, Reimink MS, Cochran RP. Annular dilatation increases stress in the mitral valve and delays coaptation: a finite element computer model. Cardiovasc Surg. 1997; 5:427–34. [PubMed: 9350801]
50. Votta E, Caiani E, Veronesi F, Soncini M, Montevecchi FM, Redaelli A. Mitral valve finite-element modelling from ultrasound data: a pilot study for a new approach to understand mitral function and clinical scenarios. Philos Trans R Soc A Math Phys Eng Sci. 2008; 366:3411–34.

51. Xu C, Brinster CJ, Jassar AS, Vergnat M, Eperjesi TJ, et al. A novel approach to in vivo mitral valve stress analysis. Am J Physiol Heart Circ Physiol. 2010; 299:H1790–94. [PubMed: 20952665]
52. Verhey JF, Nathan NS, Rienhoff O, Kikinis R, Rakebrandt F, D'Ambra MN. Finite-element-method (FEM) model generation of time-resolved 3D echocardiographic geometry data for mitral-valve volumetry. Biomed Eng Online. 2006; 5:17. [PubMed: 16512925]
53. Ryan LP, Jackson BM, Eperjesi TJ, Plappert TJ, St John-Sutton M, et al. A methodology for assessing human mitral leaflet curvature using real-time 3-dimensional echocardiography. J Thorac Cardiovasc Surg. 2008; 136:726–34. [PubMed: 18805278]
54. Wenk JF, Zhang Z, Cheng G, Malhotra D, Acevedo-Bolton G, et al. First finite element model of the left ventricle with mitral valve: insights into ischemic mitral regurgitation. Ann Thorac Surg. 2010; 89:1546–53. [PubMed: 20417775]
55. Stevanella M, Krishnamurthy G, Votta E, Swanson JC, Redaelli A, Ingels NB Jr. Mitral leaflet modeling: importance of in vivo shape and material properties. J Biomech. 2011; 44:2229–35. [PubMed: 21704316]
56. Stevanella M, Maffessanti F, Conti CA, Votta E, Arnoldi A, et al. Mitral valve patient-specific finite element modeling from cardiac MRI: application to an annuloplasty procedure. Cardiovasc Eng Technol. 2011; 2:66–76.
57. Wang Q, Book G, Contreras Ortiz S, Primiano C, McKay R, et al. Dimensional analysis of aortic root geometry during diastole using 3D models reconstructed from clinical 64-slice computed tomography images. Cardiovasc Eng Technol. 2011; 2:324–33.
58. Wang Q, Sirois E, Sun W. Patient-specific modeling of biomechanical interaction in transcatheter aortic valve deployment. J Biomech. 2012; 45:1965–71. [PubMed: 22698832]
59. Sirois E, Wang Q, Sun W. Fluid simulation of a transcatheter aortic valve deployment into a patient-specific aortic root. Cardiovasc Eng Technol. 2011; 2:186–95.
60. Capelli C, Bosi GM, Cerri E, Nordmeyer J, Odenwald T, et al. Patient-specific simulations of transcatheter aortic valve stent implantation. Med Biol Eng Comput. 2012; 50:183–92. [PubMed: 22286953]
61. Pouch AM, Xu C, Yushkevich PA, Jassar AS, Vergnat M, et al. Semi-automated mitral valve morphometry and computational stress analysis using 3D ultrasound. J Biomech. 2012; 45:903–7. [PubMed: 22281408]
62. Pouch, A., Wang, H., Takabe, M., Jackson, B., Sehgal, C., et al. Automated segmentation and geometrical modeling of the tricuspid aortic valve in 3D echocardiographic images. In: Mori, K.Sakuma, I.Sato, Y.Barillot, C., Navab, N., editors. Medical Image Computing and Computer-Assisted Intervention—MICCAI 2013. Vol. 8149. Berlin: Springer; 2013. p. 485-92.LNCS
63. Zheng Y, John M, Liao R, Nöttling A, Boese J, et al. Automatic aorta segmentation and valve landmark detection in C-arm CT for transcatheter aortic valve implantation. IEEE Trans Med Imaging. 2012; 31:2307–21. [PubMed: 22955891]
64. Nie, Y., Luo, Z., Cai, J., Gu, L. A novel aortic valve segmentation from ultrasound image using continuous max-flow approach. Proc. 35th Annu. Int. Conf. IEEE Eng. Med. Biol. Soc. (EMBC); Osaka, Japan. 2013. p. 3311-14.
65. Dong, B., Guo, Y., Wang, B., Gu, L. Aortic valve segmentation from ultrasound images based on shape constraint CV model. Proc. 35th Annu. Int. Conf. IEEE Eng. Med. Biol. Soc. (EMBC); Osaka, Japan. 2013. p. 1402-5.
66. Ionasec RI, Voigt I, Georgescu B, Yang W, Houle H, et al. Patient-specific modeling and quantification of the aortic and mitral valves from 4D cardiac CT and TEE. IEEE Trans Med Imaging. 2010; 29:1636–51. [PubMed: 20442044]
67. Veronesi F, Corsi C, Sugeng L, Mor-Avi V, Caiani EG, et al. A study of functional anatomy of aortic-mitral valve coupling using 3D matrix transesophageal echocardiography. Circ Cardiovasc Imaging. 2009; 2:24–31. [PubMed: 19808561]
68. May-Newman K, Yin FC. Biaxial mechanical behavior of excised porcine mitral valve leaflets. Am J Physiol. 1995; 269:H1319–27. [PubMed: 7485564]
69. Kunzelman KS, Cochran RP. Stress/strain characteristics of porcine mitral valve tissue: parallel versus perpendicular collagen orientation. J Card Surg. 1992; 7:71–78. [PubMed: 1554980]

70. Grashow JS, Yoganathan AP, Sacks MS. Biaixal stress–stretch behavior of the mitral valve anterior leaflet at physiologic strain rates. Ann Biomed Eng. 2006; 34:315–25. [PubMed: 16450193]
71. He Z, Ritchie J, Grashow JS, Sacks MS, Yoganathan AP. In vitro dynamic strain behavior of the mitral valve posterior leaflet. J Biomech Eng. 2005; 127:504–11. [PubMed: 16060357]
72. He Z, Sacks MS, Baijens L, Wanant S, Shah P, Yoganathan AP. Effects of papillary muscle position on in-vitro dynamic strain on the porcine mitral valve. J Heart Valve Dis. 2003; 12:488–94. [PubMed: 12918852]
73. Sacks MS, Enomoto Y, Graybill JR, Merryman WD, Zeeshan A, et al. In-vivo dynamic deformation of the mitral valve anterior leaflet. Ann Thorac Surg. 2006; 82:1369–77. [PubMed: 16996935]
74. Sacks MS, He Z, Baijens L, Wanant S, Shah P, et al. Surface strains in the anterior leaflet of the functioning mitral valve. Ann Biomed Eng. 2002; 30:1281–90. [PubMed: 12540204]
75. Chen L, Yin FCP, May-Newman K. The structure and mechanical properties of the mitral valve leaflet-strut chordae transition zone. J Biomech Eng. 2004; 126:244–51. [PubMed: 15179855]
76. Lo D, Vesely I. Biaxial strain analysis of the porcine aortic valve. Ann Thorac Surg. 1995; 69:S374–78.
77. Billiar KL, Sacks MS. Biaxial mechanical properties of the natural and glutaraldehyde treated aortic valve cusp—part I: experimental results. J Biomech Eng. 2000; 122:23–30. [PubMed: 10790826]
78. Stephens EH, Grande-Allen KJ. Age-related changes in collagen synthesis and turnover in porcine heart valves. J Heart Valve Dis. 2007; 16:672–82. [PubMed: 18095519]
79. Nicosia MA, Kasalko JS, Cochran RP, Einstein DR, Kunzelman KS. Biaxial mechanical properties of porcine ascending aortic wall tissue. J Heart Valve Dis. 2002; 11:680–87. [PubMed: 12358405]
80. Auricchio F, Conti M, Morganti S, Reali A. Simulation of transcatheter aortic valve implantation: a patient-specific finite element approach. Comput Methods Biomech Biomed Eng. 2014; 17:1347–57.
81. Weinberg EJ, Kaazempur Mofrad MR. A finite shell element for heart mitral valve leaflet mechanics, with large deformations and 3D constitutive material model. J Biomech. 2007; 40:705–11. [PubMed: 16574127]
82. Krishnamurthy G, Itoh A, Bothe W, Swanson JC, Kuhl E, et al. Stress–strain behavior of mitral valve leaflets in the beating ovine heart. J Biomech. 2009; 42:1909–16. [PubMed: 19535081]
83. Stevanella M, Votta E, Redaelli A. Mitral valve finite element modeling: Implications of tissues' nonlinear response and annular motion. J Biomech Eng. 2009; 131:121010. [PubMed: 20524733]
84. Prot V, Haaverstad R, Skallerud B. Finite element analysis of the mitral apparatus: annulus shape effect and chordal force distribution. Biomech Model Mechanobiol. 2009; 8:43–55. [PubMed: 18193309]
85. Rausch MK, Bothe W, Kvitting JPE, Göktepe S, Miller DC, Kuhl E. In vivo dynamic strains of the ovine anterior mitral valve leaflet. J Biomech. 2011; 44:1149–57. [PubMed: 21306716]
86. Krishnamurthy G, Ennis DB, Itoh A, Bothe W, Swanson JC, et al. Material properties of the ovine mitral valve anterior leaflet in vivo from inverse finite element analysis. Am J Physiol Heart Circ Physiol. 2008; 295:H1141–49. [PubMed: 18621858]
87. Clark RE. Stress-strain characteristics of fresh and frozen human aortic and mitral leaflets and chordae tendineae: implications for clinical use. J Thorac Cardiovasc Surg. 1973; 66:202–8. [PubMed: 4720973]
88. Pham T, Sun W. Material properties of aged human mitral valve leaflets. J Biomed Mater Res Part A. 2013; In press. doi: 10.1002/jbm.a.34939
89. Pham T, Sun W. Comparison of biaxial mechanical properties of coronary sinus tissues from porcine, ovine and aged human species. J Mech Behav Biomed Mater. 2012; 6:21–29. [PubMed: 22301170]
90. Mummert J, Sirois E, Sun W. Quantification of biomechanical interaction of transcatheter aortic valve stent deployed in porcine and ovine hearts. Ann Biomed Eng. 2013; 41:577–86. [PubMed: 23161165]

91. Votta E, Maisano F, Bolling SF, Alfieri O, Montevecchi FM, Redaelli A. The Geoform disease-specific annuloplasty system: a finite element study. Ann Thorac Surg. 2007; 84:92–101. [PubMed: 17588392]
92. Fung, YC. Biomechanics: Mechanical Properties of Living Tissues. New York: Springer; 1993.
93. Humphrey, JD. Cardiovascular Solid Mechanics: Cells, Tissues, and Organs. New York: Springer; 2002.
94. Sun W, Abad A, Sacks MS. Simulated bioprosthetic heart valve deformation under quasi-static loading. J Biomech Eng. 2005; 127:905–14. [PubMed: 16438226]
95. Sacks MS, Sun W. Multiaxial mechanical behavior of biological materials. Annu Rev Biomed Eng. 2003; 5:251–84. [PubMed: 12730082]
96. Sun W, Sacks MS. Finite element implementation of a generalized Fung-elastic constitutive model for planar soft tissues. Biomech Model Mechanobiol. 2005; 4:190–99. [PubMed: 16075264]
97. Weiss JA, Maker BN, Govindjee S. Finite element implementation of incompressible, transversely isotropic hyperelasticity. Comput Methods Appl Mech Eng. 1996; 135:107–28.
98. Holzapfel GA, Gasser TC, Ogden RW. A new constitutive framework for arterial wall mechanics and a comparative study of material models. J Elasticity. 2000; 61:1–48.
99. May-Newman K, Yin FC. A constitutive law for mitral valve tissue. J Biomech Eng. 1998; 120:38–47. [PubMed: 9675679]
100. Conti CA, Votta E, Della Corte A, Del Viscovo L, Bancone C, et al. Dynamic finite element analysis of the aortic root from MRI-derived parameters. Med Eng Phys. 2010; 32:212–21. [PubMed: 20060766]
101. Gould PL, Cataloglu A. Stress analysis of the human aortic valve. Comput Struct. 1973; 3:377–78. IN1–2, 379–84.
102. Cataloglu A, Gould PL, Clark RE. Validation of a simplified mathematical model for the stress analysis of human aortic heart valves. J Biomech. 1975; 8:347–48. [PubMed: 1184606]
103. Leat ME, Fisher J. The influence of manufacturing methods on the function and performance of a synthetic leaflet heart valve. Proc Inst Mech Eng H. 1995; 209:65–69. [PubMed: 7669122]
104. Leat ME, Fisher J. A synthetic leaflet heart valve with improved opening characteristics. Med Eng Phys. 1994; 16:470–76. [PubMed: 7858778]
105. Cacciola G, Peters GW, Baaijens FP. A synthetic fiber-reinforced stentless heart valve. J Biomech. 2000; 33:653–58. [PubMed: 10807985]
106. Cacciola G, Peters GW, Schreurs PJ. A three-dimensional mechanical analysis of a stentless fibre-reinforced aortic valve prosthesis. J Biomech. 2000; 33:521–30. [PubMed: 10708772]
107. Krucinski S, Vesely I, Dokainish MA, Campbell G. Numerical simulation of leaflet flexure in bioprosthetic valves mounted on rigid and expansile stents. J Biomech. 1993; 26:929–43. [PubMed: 8349718]
108. Martin C, Sun W. Simulation of long-term fatigue damage in bioprosthetic heart valves: effect of leaflet and stent elastic properties. Biomech Model Mechanobiol. 2013; doi: 10.1007/s10237-013-0532-x
109. David TE, Feindel CM. An aortic valve-sparing operation for patients with aortic incompetence and aneurysm of the ascending aorta. J Thorac Cardiovasc Surg. 1992; 103:617–22. [PubMed: 1532219]
110. Soncini M, Votta E, Zinicchino S, Burrone V, Mangini A, et al. Aortic root performance after valve sparing procedure: a comparative finite element analysis. Med Eng Phys. 2009; 31:234–43. [PubMed: 18786848]
111. Totaro P, Morganti S, Ngo Yon C, Dore R, Conti M, et al. Computational finite element analyses to optimize graft sizing during aortic valve-sparing procedure. J Heart Valve Dis. 2012; 21:141–47. [PubMed: 22645846]
112. Ranga A, Bouchot O, Mongrain R, Ugolini P, Cartier R. Computational simulations of the aortic valve validated by imaging data: evaluation of valve-sparing techniques. Interact Cardiovasc Thorac Surg. 2006; 5:373–78. [PubMed: 17670596]
113. Beck A, Thubrikar M, Robicsek F. Stress analysis of the aortic valve with and without the sinuses of Valsalva. J Heart Valve Dis. 2001; 10:1–11. [PubMed: 11206754]

114. Nicosia MA, Cochran RP, Einstein DR, Rutland CJ, Kunzelman KS. A coupled fluid-structure finite element model of the aortic valve and root. J Heart Valve Dis. 2003; 12:781–89. [PubMed: 14658821]
115. Marom G, Peleg M, Halevi R, Rosenfeld M, Raanani E, et al. Fluid-structure interaction model of aortic valve with porcine-specific collagen fiber alignment in the cusps. J Biomech Eng. 2013; 135:101001. [PubMed: 23775457]
116. Kunzelman KS, Quick DW, Cochran RP. Altered collagen concentration in mitral valve leaflets: biochemical and finite element analysis. Ann Thorac Surg. 1998; 66:S198–205. [PubMed: 9930448]
117. Reimink MS, Kunzelman KS, Verrier ED, Cochran RP. The effect of anterior chordal replacement on mitral valve function and stresses: a finite element study. ASAIO J. 1995; 41:M754–62. [PubMed: 8573908]
118. Reimink MS, Kunzelman KS, Cochran RP. The effect of chordal replacement suture length on function and stresses in repaired mitral valves: a finite element study. J Heart Valve Dis. 1996; 5:365–75. [PubMed: 8858500]
119. Maisano F, Redaelli A, Soncini M, Votta E, Arcobasso L, Alfieri O. An annular prosthesis for the treatment of functional mitral regurgitation: finite element model analysis of a dog bone-shaped ring prosthesis. Ann Thorac Surg. 2005; 79:1268–75. [PubMed: 15797061]
120. Wong VM, Wenk JF, Zhang Z, Cheng G, Acevedo-Bolton G, et al. The effect of mitral annuloplasty shape in ischemic mitral regurgitation: a finite element simulation. Ann Thorac Surg. 2012; 93:776–82. [PubMed: 22245588]
121. Xu C, Jassar AS, Nathan DP, Eperjesi TJ, Brinster CJ, et al. Augmented mitral valve leaflet area decreases leaflet stress: a finite element simulation. Ann Thorac Surg. 2012; 93:1141–45. [PubMed: 22397985]
122. Itoh A, Krishnamurthy G, Swanson JC, Ennis DB, Bothe W, et al. Active stiffening of mitral valve leaflets in the beating heart. Am J Physiol Heart Circ Physiol. 2009; 296:H1766–73. [PubMed: 19363135]
123. Skallerud B, Prot V, Nordrum IS. Modeling active muscle contraction in mitral valve leaflets during systole: a first approach. Biomech Model Mechanobiol. 2011; 10:11–26. [PubMed: 20419330]
124. Boekstegers P, Hausleiter J, Baldus S, Von Bardeleben RS, Beucher H, et al. Percutaneous interventional mitral regurgitation treatment using the Mitra-Clip system. Clin Res Cardiol. 2013; 103:85–96.
125. Redaelli A, Guadagni G, Fumero R, Maisano F, Alfieri O. A computational study of the hemodynamics after “edge-to-edge” mitral valve repair. J Biomech Eng. 2001; 123:565–70. [PubMed: 11783727]
126. Fiore, GB., Guadagni, G., Putignano, G., Redaelli, A., Fumero, R., et al. Experimental and computational simulation of the haemodynamic conditions after edge-to-edge mitral valve repair. Proc Bioengineering Conference; Snowbird, UT. New York: Am. Soc. Mech. Eng., Bioeng. Div; 2001. p. 429-30.
127. Votta E, Maisano F, Soncini M, Redaelli A, Montevecchi FM, Alfieri O. 3-D computational analysis of the stress distribution on the leaflets after edge-to-edge repair of mitral regurgitation. J Heart Valve Dis. 2002; 11:810–22. [PubMed: 12479282]
128. Avanzini A. A computational procedure for prediction of structural effects of edge-to-edge repair on mitral valve. J Biomech Eng. 2008; 130:031015. [PubMed: 18532864]
129. Lau KD, Díaz-Zuccarini V, Scambler P, Burriesci G. Fluid–structure interaction study of the edge-to-edge repair technique on the mitral valve. J Biomech. 2011; 44:2409–17. [PubMed: 21767842]
130. Dal Pan F, Donzella G, Fucci C, Schreiber M. Structural effects of an innovative surgical technique to repair heart valve defects. J Biomech. 2005; 38:2460–71. [PubMed: 16214494]
131. Ma X, Gao H, Griffith BE, Berry C, Luo X. Image-based fluid–structure interaction model of the human mitral valve. Comput Fluids. 2013; 71:417–25.

132. Dahl SK, Vierendeels J, Degroote J, Annerel S, Hellevik LR, Skallerud B. FSI simulation of asymmetric mitral valve dynamics during diastolic filling. Comput Methods Biomech Biomed Eng. 2012; 15:121–30.
133. Martin C, Sun W, Primiano C, McKay R, Elefteriades J. Age-dependent ascending aorta mechanics assessed through multiphase CT. Ann Biomed Eng. 2013; 41:2565–74. [PubMed: 23817767]
134. Gee MW, Reeps C, Eckstein HH, Wall WA. Prestressing in finite deformation abdominal aortic aneurysm simulation. J Biomech. 2009; 42:1732–39. [PubMed: 19457489]
135. Lu J, Zhou X, Raghavan ML. Inverse method of stress analysis for cerebral aneurysms. Biomech Model Mechanobiol. 2008; 7:477–86. [PubMed: 17990015]
136. Zhou X, Raghavan ML, Harbaugh RE, Lu J. Patient-specific wall stress analysis in cerebral aneurysms using inverse shell model. Ann Biomed Eng. 2010; 38:478–89. [PubMed: 19953324]
137. Wang, Q., Kodali, S., Sun, W. Analysis of aortic root rupture during transcatheter aortic valve implantation using computational simulations. Presented at 12th US Natl. Congr. Comput. Mech. (USNCCM12); July 22–25; Raleigh, NC. 2013.
138. Thacker BH, Riha DS, Fitch SHK, Huyse LJ, Pleming JB. Probabilistic engineering analysis using the NESSUS software. Struct Saf. 2006; 28:83–107.
139. Baldwin MA, Laz PJ, Stowe JQ, Rullkoetter PJ. Efficient probabilistic representation of tibiofemoral soft tissue constraint. Comput Methods Biomech Biomed Eng. 2009; 12:651–59.
140. Laz PJ, Pal S, Fields A, Petrella AJ, Rullkoetter PJ. Effects of knee simulator loading and alignment variability on predicted implant mechanics: a probabilistic study. J Orthop Res. 2006; 24:2212–21. [PubMed: 17004268]
141. Laz PJ, Pal S, Halloran JP, Petrella AJ, Rullkoetter PJ. Probabilistic finite element prediction of knee wear simulator mechanics. J Biomech. 2006; 39:2303–10. [PubMed: 16185700]
142. Pal S, Langenderfer JE, Stowe JQ, Laz PJ, Petrella AJ, Rullkoetter PJ. Probabilistic modeling of knee muscle moment arms: effects of methods, origin-insertion, and kinematic variability. Ann Biomed Eng. 2007; 35:1632–42. [PubMed: 17546504]
143. Li, K., Sun, W. Probabilistic computational analysis of transcatheter aortic valve leaflet design. Proc. ASME 2013 Summer Bioeng. Conf; June 26–29; Sunriver, OR. 2013. SBC2013-14418
144. Weinberg EJ, Shahmirzadi D, Mofrad MRK. On the multiscale modeling of heart valve biomechanics in health and disease. Biomech Model Mechanobiol. 2010; 9:373–87. [PubMed: 20066464]
145. Huang HYS, Liao J, Sacks MS. In-situ deformation of the aortic valve interstitial cell nucleus under diastolic loading. J Biomech Eng. 2007; 129:880–89. [PubMed: 18067392]
146. Vesely I, Noseworthy R. Micromechanics of the fibrosa and the ventricularis in aortic valve leaflets. J Biomech. 1992; 25:101–13. [PubMed: 1733978]
147. Weinberg EJ, Mofrad MRK. Three-dimensional, multiscale simulations of the human aortic valve. Cardiovasc Eng. 2007; 7:140–55. [PubMed: 18026835]
148. Weinberg EJ, Kaazempur Mofrad MR. A multiscale computational comparison of the bicuspid and tricuspid aortic valves in relation to calcific aortic stenosis. J Biomech. 2008; 41:3482–87. [PubMed: 18996528]

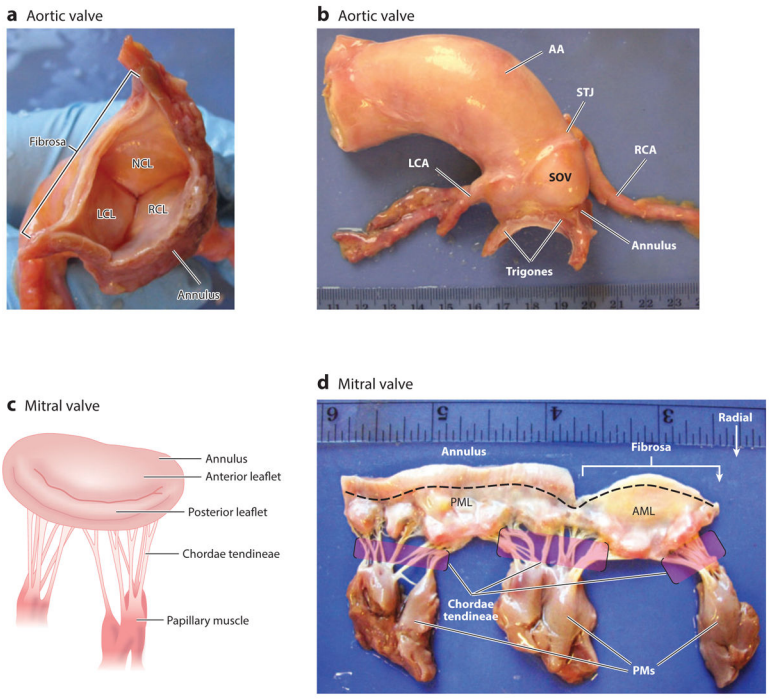

Figure 1.

Photographs of the structure of an excised human aortic root showing (*a*) the entire circumference of the annulus composed of fibrous and muscular regions and the coapting aortic leaflets—that is, the noncoronary (NCL), left coronary (LCL), and right coronary leaflets (RCL)—and (*b*) the same aortic root with the ascending aorta (AA), right (RCA) and left coronary arteries (LCA), noncoronary sinus of Valsalva (SOV), sinotubular junction (STJ), and trigone regions. (*c*) An illustration of the mitral valve anatomical structures, and (*d*) a photograph of an excised human mitral valve showing the mitral annulus, anterior (AML) and posterior mitral leaflets (PML), fibrous region, chordae tendineae (*pink highlighted area*), and papillary muscles (PMs).

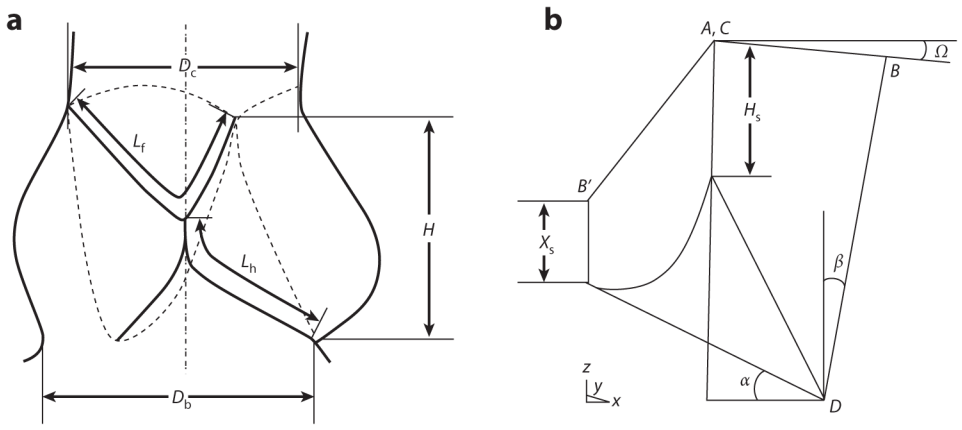

Figure 2.

(*a*) Drawing of the aortic valve showing a side view of one leaflet. (*b*) Schematic showing the side view of one leaflet in both the open and closed valve positions. Points A and C indicate the top of the commissures, point B (B′) indicates the middle point of the leaflet free edge in the open (closed) position, and point D indicates the middle point of the leaflet attachment line. Abbreviations: D_b, diameter of the base; D_c, diameter of the commissures; H, valve height; H_s, height of the commissures; L_f, leaflet free-edge length; L_h, leaflet height; X_s, coaptation height in the center of the valve; α, angle of the closed valve; β, angle of the open valve; Ω, angle of the leaflet free edge in the open position. [Adapted with permission from Labrosse et al. (43).]

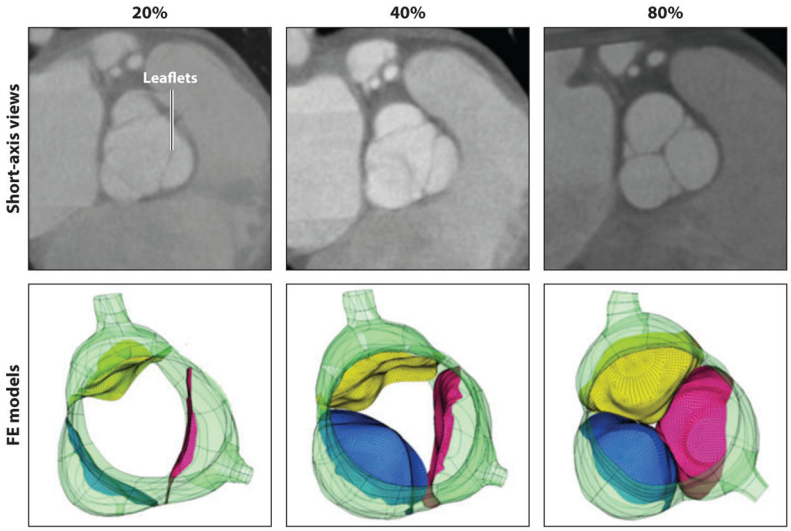

Figure 3.

(*top*) Short-axis views of patient aortic valve computed tomography (CT) images at 20% (fully opened), 40%(half opened), and 80% (fully closed) of a cardiac cycle. (*bottom*) The corresponding reconstructed three-dimensional aortic root and leaflet finite element (FE) models showing fully opened, half-opened, and fully closed valve geometries (*left to right*).

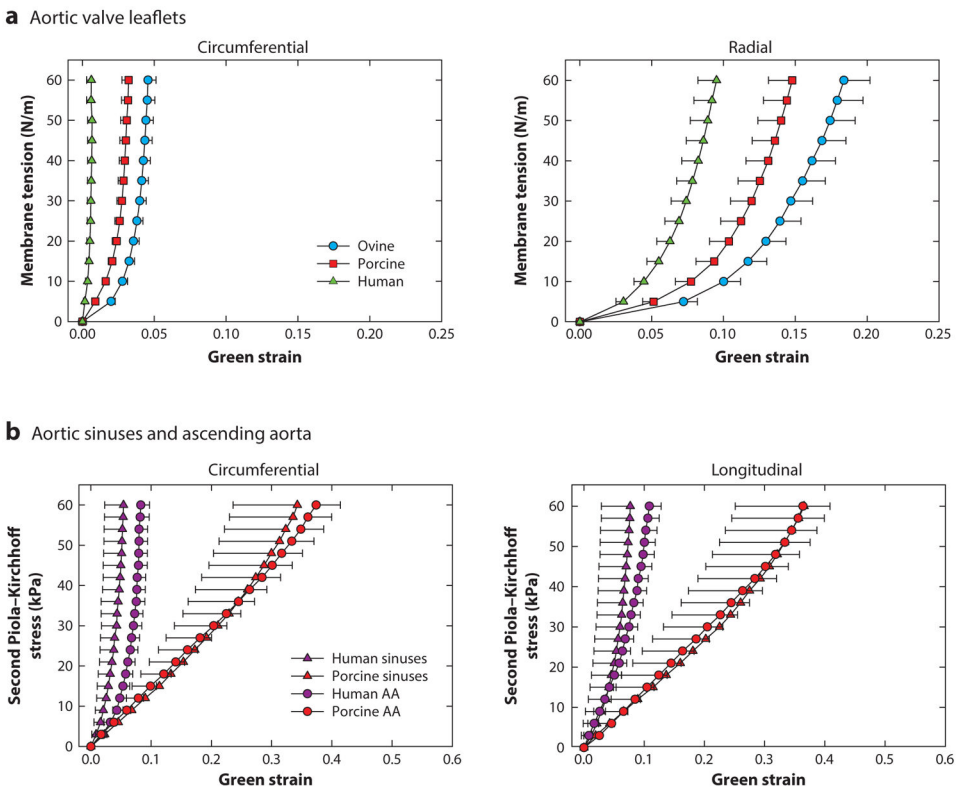

Figure 4.

Mean experimental biaxial response curves of (*a*) ovine, porcine, and human aortic leaflets in circumferential and radial directions and (*b*) porcine and ovine aortic sinuses and ascending aorta (AA) in circumferential and longitudinal directions.

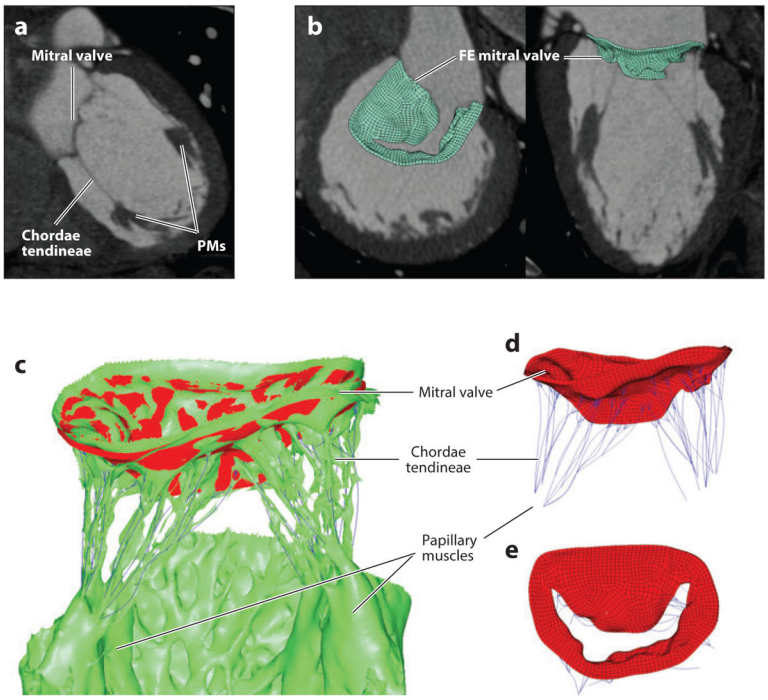

Figure 5.

A three-dimensional finite element (FE) mitral valve (MV) model. (*a*) The computed tomography (CT) long-axis two-chamber view of a closed MV showing a good visualization of chordae tendineae and papillary muscles (PMs). (*b*) The short-axis and long-axis views of the reconstructed FE MV model overlapped with the CT images. (*c*) The overlapping of geometries of the closed MV valve from the CT scans (*green*) and the simulated result (*red*) after applied pressure demonstrate a good match. Open MV valve geometry and the anatomical locations of chordae tendineae with chordal origins and papillary muscles are shown in (*d*) long-axis and (*e*) short-axis views.

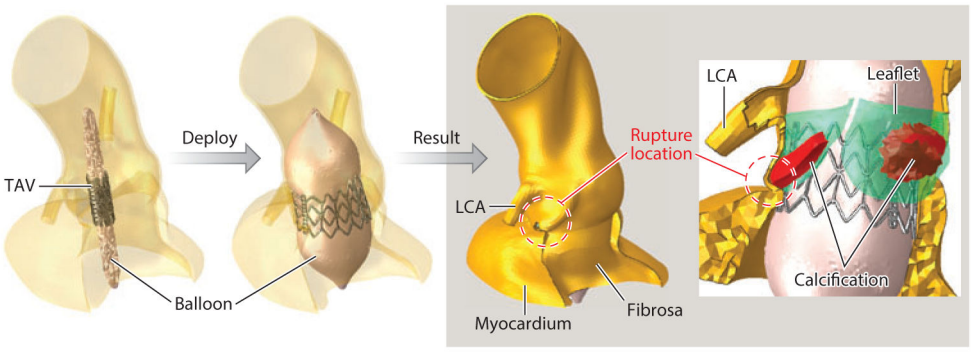

Figure 6.

A finite element model of a 94-year-old patient's aorta, including the entire aortic root with coronary arteries, calcified leaflets, and a balloon-expandable transcatheter aortic valve (TAV) device. The simulation results predicted the aortic sinus rupture below the left coronary artery (LCA), which matched clinical observation.